



Direct-micro-fabrication of Hydrophobic Surface with Re-entrant Texture on Metal Produced by Femtosecond-pulsed Laser

Masaki Yamaguchi¹ · Shunichi Kato¹

Accepted: 24 November 2022 / Published online: 29 November 2022
© The Author(s) 2022

Abstract

Re-entrant textures are promising geometries for hydrophobic surfaces, however a direct processing method of microscale re-entrant textures applicable for general industrial materials such as metals has yet to be established. The purpose of this study was to demonstrate a possibility of direct processing method of microscale re-entrant textures by using a femtosecond-pulsed laser. We designed a novel and simple optical unit including a pair of step mirrors and a newly designed aspherical condenser lens that enable processing of reverse-tapered uniaxial grooves. A maximum reverse-taper angle of 20° was achieved on stainless steel using a femtosecond-pulsed laser that could be controlled linearly with the step mirror angles. Four types of test-pieces with re-entrant texture composed of reverse-tapered grooves were fabricated with reverse-tapered angles of $5 - 20^\circ$. It was demonstrated that the apparent contact angle exhibited an increase in the processed angle of the re-entrant texture. The re-entrant structures on stainless steel achieved a hydrophobicity over 140° of apparent contact angle with good stability, and allowing water droplets to slide off.

Keywords Femtosecond-pulsed laser · Re-entrant texture · Reverse-tapered groove · Direct microfabrication · Hydrophobicity

Introduction

It has been pointed out by Herminghaus [1] that the various surface constituents of leaves of numerous plants, such as the common smoketree or wild cabbage, have superhydrophobic surfaces that are expected to be due to re-entrant texture [2, 3]. The re-entrant surface curvature can be used to design surfaces with extreme

✉ Masaki Yamaguchi
masakiy@shinshu-u.ac.jp
<http://fiber.shinshu-u.ac.jp/yamaguchi/TOP.html>

¹ Graduate School of Medicine, Science & Technology, Shinshu University, 3-15-1 Tokida, Nagano 386-8567 Ueda, Japan

resistance to wetting for multiple kinds of liquids with low surface tension. A critical parameter of re-entrant texture is the angle formed between the sidewalls of the indent and the horizontal line [4, 5]. The reverse-taper angle is defined as the angle made clockwise from the vertical line at the center of the hole (Fig. 1). The micro-periodic structure has a geometry such as width of the solid–liquid interface, f_1 (=tooth width), width of the liquid–air interface, f_2 (=groove width), pitch, τ ($=f_1+f_2$), and depth, d . In a forward-tapered hole, the angle of the convex top is larger than the angle of the indent bottom. Conversely, in a reverse-tapered hole, the angle of the convex top is smaller than the angle of the indent bottom. The latter shape can form the re-entrant texture. Increasing the reverse-taper would enhance the ability of asperities to suspend drops [6–8]. For re-entrant curved surfaces, the net traction on the liquid–vapor interface is directed upwards, thereby supporting the formation of a composite interface. Additionally, four design criteria have been proposed to form an air-entrapped Cassie–Baxter state from the re-entrant texture considering the pressure balance of liquids, such as Laplace pressure, gravity, surface curvature, pinning effects, and the suspending conditions [9].

Several fabrication methods have been proposed to process re-entrant textures, such as lithographic techniques [10, 11], nanoimprinting [12, 13], reactive ion etching [14], spin coating [15], self-assembly [16], and laser [17, 18]. Kang and Choi created mushroom-like micropillar arrays by photolithography on silicon [10]. Yun et al. assembled primary doubly re-entrant nanostructures on secondary microgrooves by nanoimprinting [12]. An overhang structure fabricated by using reverse nanoimprint lithography was used in conjunction with reactive ion etching as a re-entrant texture [14]. An oleophobic surface was fabricated by spin coating with ultra-violet-cure resin and poly(tetrafluoroethylene) microbeads [15]. Mushroom-like microstructures were fabricated by self-assembly and dip-coating using magnetic particles [16]. A fabrication process using laser ablation and electrodeposition was also investigated [17]. Yang et al. proposed a laser-induced self-growing mushroom-like microstructure on poly(ethylene terephthalate) tape/heat-shrinkable polystyrene bilayer surfaces [18]. However, with these processing methods, materials were limited to silicon and resin, and no method existed that can process any

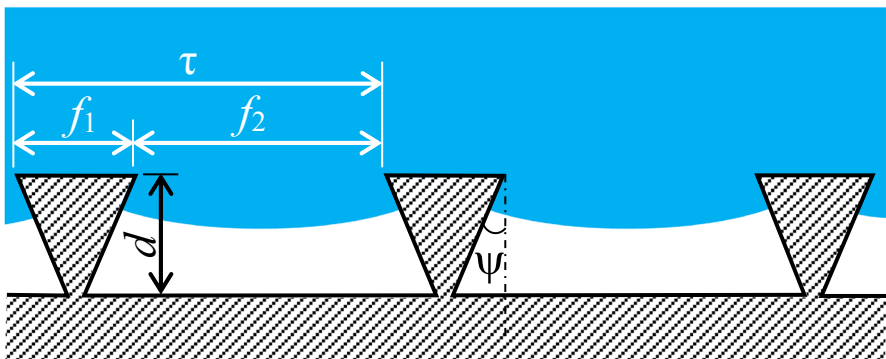


Fig. 1 Geometries of a re-entrant texture with reverse-taper angle, ψ

materials. A direct processing method of microscale re-entrant texture that applicable for general industrial materials such as metals has yet to be established.

To overcome the limitations, we focused on pulsed laser sources as a direct processing method of microscale re-entrant texture on metals. Femtosecond-pulsed lasers have been applied for three-dimensional processing with nano- and micro-scale surface topography in an open environment and in an acceptable time for multiple materials [19, 20]. The processing angle that can be applicable to overhang processing have been especially used in interference laser processing [21]. Since the conception of the Mach–Zehnder interferometer, numerous types of beam correlators such as Lloyd’s mirror and the transmission beam splitter with Schwarzschild optics have been used for laser interference patterning [22]. Fan et al. improved the taper degree of laser-drilled holes by adopting a nanosecond double-pulse laser beam [23]. However, these processing methods rarely have reverse-taper angle that exceeds 10° , which may be because no need existed for such processing on the surface of materials.

The purpose of this study was to demonstrate a possibility of direct processing method of microscale re-entrant textures by using a femtosecond-pulsed laser. We designed a novel and simple optical unit for reverse-taper processing including a pair of step mirrors and a newly designed aspherical condenser lens. We optimized the reverse-taper angle of uniaxial grooves through femtosecond-pulsed laser processing of stainless steel and evaluated the characteristics of the proposed optical unit. Subsequently, we evaluated the geometries of re-entrant texture composed of reverse-tapered uniaxial grooves. Finally, we demonstrated the hydrophobicity of re-entrant texture made on stainless steel.

Materials and Methods

Principle of Optical Unit for Reverse-Taper Processing

An optical unit for processing reverse-tapered uniaxial grooves comprised (i) a beam expander ($\times 1/4$, BEZHP-2/8–500/570, Sigmakoki Co., Ltd., Tokyo, Japan), (ii) a pair of step mirrors (0.008° of resolution of stepping motor, Suruga Seiki Co., Ltd., Shizuoka, Japan), (iii) a fixed mirror, and (iv) an aspherical condenser lens (Fig. 2). The aspherical condenser lens (synthetic quartz) was designed by the authors to meet the following specifications: 20° of irradiation angle after passing, 24 mm of effective diameter, 15.0 mm of thickness, and 17.14 mm of focal length, and manufactured by a company (Natsume Optical Co., Iida, Japan). An x – y electric-stage (HST-50X, $2\ \mu\text{m}$ of repeated positioning accuracy, Sigmakoki Co., Ltd.), a dual-directions (x – y) tilt stage (KRE04360-C, 0.00034° of resolution, Kohzu Precision Co., Ltd., Japan), and a z -stage (OSMS60-10ZF, $5\ \mu\text{m}$ of repeated positioning accuracy, Sigmakoki Co., Ltd.) were installed on a table on which a work piece was placed. Prior to the experiment, the test piece was levelled by using a digital level meter (SELN-011B, Sakamoto Electric MFG Co., Ltd., Fukuoka, Japan) to satisfy within 0.001° and the focal length was set to a target value. A commercial femtosecond-pulsed laser (Pharos-6 W, Light

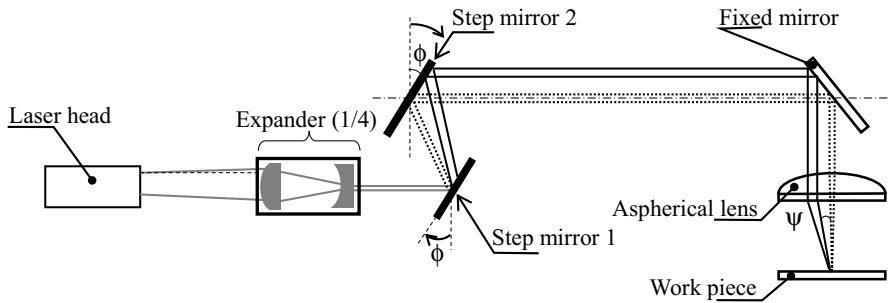


Fig. 2 Designed optical unit for reverse-taper processing with a femtosecond pulsed laser

Conversion UAB, Vilnius, Republic of Lithuania) providing pulses at an oscillatory wavelength of 515 nm, a pulse width of 277 fs, and a repetition rate of 10 kHz was used for this experiment.

The distance of a laser beam from the centre of the aspherical condenser lens was controlled by changing the angle of the step mirrors (ϕ). A processing angle (irradiation angle with respect to the workpiece, ψ) is determined according to this distance of a laser beam from the center of the aspherical condenser lens. After that, a reverse-tapered uniaxial groove was processed when the laser beam scanned in one direction (uniaxial groove processing in x -direction).

Characteristics of Optical Unit for Reverse-Taper Processing

Stainless steel (SUS304, JIS G 4305, 30 mm \times 30 mm of area and 1 mm of thickness, $R_a = 6.3 \mu\text{m}$ of surface roughness (without polish), Nippon Steel Stainless Steel Co., Tokyo, Japan) was used for fabricating test-pieces. The surface roughness was measured using a non-contact laser confocal microscope (10 nm resolution for depth, OLS4100, Olympus Co., Tokyo, Japan). In order to determine the relationship between step mirror angle and processed angle, the side-views of the reverse-tapered uniaxial grooves were observed using the x - y electric-stage. The pulse-to-pulse overlap (overlap ratio, OR) was calculated as a function of the pulse separation distance, p , and the spot diameter, D , as follows [24]:

$$OR = \left(1 - \frac{p}{D}\right) \cdot 100\% \quad (1)$$

The parameters were fluence, F , at $250 \text{ mJ}/\text{mm}^2$ and overlap ratio, OR , at 99.6%. In this evaluation, the test-pieces were placed at the focal position in the depth direction, z , where the diameter of the processing mark was smallest. Where, $250 \text{ mJ}/\text{mm}^2$ of fluence was the upper limit of our processing system. This was performed by using the z -stage and was defined as $0 \mu\text{m}$. The spot diameter, D , at the focal position on the test-piece surface was calculated to be $11.6 \mu\text{m}$ by $1/e^2$ using the

focal length of the focusing lens $f = 17.14$ mm, a laser beam quality with $M^2 = 1.117$, and an expanded (1/4) laser beam diameter $d_b = 4.83$ mm as follows [25]:

$$D = \frac{4f\lambda M^2}{\pi d_b} \quad \mu\text{m} \quad (2)$$

The spot diameter was set to achieve processing resolution in 10 μm scales.

Optimization of Laser Processing

The optimum processing conditions were identified based on the shape of perpendicularly uniaxial groove processing. The micro-periodic structure has a geometry such as f_1 (=tooth width), f_2 (=groove width), τ ($=f_1 + f_2$), and d (please see Supplementary Materials Section for further details). The relationship between the depth and the shot number was measured at 250 mJ/mm^2 of fluence and 80% of the overlap ratio with perpendicularly uniaxial groove processing. The surface and side geometries of the test-pieces were observed using the non-contact laser confocal microscope. Prior to side observation of reverse-taper angles of re-entrant textures, the edge surface was polished using a polishing sheet (#8000 defined by ISO 8486–2:2007, Riken Corundum Co., Ltd., Saitama, Japan).

Fabrication of Re-Entrant Texture

Three processed angles of 0° , $+20^\circ$, and -20° were repeated at the same position for each angle in order to construct a re-entrant texture in 3 $\text{mm} \times 3$ mm of processing area using the x - y electric-stage. Test-pieces with re-entrant textures were fabricated at 250 mJ/mm^2 of fluence and 80% of the overlap ratio, with the uniaxial groove processing. Finally, four types of test-pieces with re-entrant textures at reverse-tapered angles of 5, 10, 15, and 20° were prepared under the optimal conditions such as 250 mJ/mm^2 of fluence, 80% of the overlap ratio.

Measurement of Apparent Contact Angle and Sliding Characteristics

The apparent contact angles, θ' , of the test-pieces with re-entrant textures were measured using a commercial contact angle analyzer (DM-701, Kyowa Interface Science Co. Ltd., Japan) by dropping 2 μL of distilled water droplet from a microsyringe at 24 $^\circ\text{C}$. The measurements were repeated five times ($n=5$), and the mean values were used.

Finally, the sliding angles, α , were observed by dropping 12 μL of distilled water droplet. For this evaluation, we used a test-piece of the reverse-tapered uniaxial groove with a width of 5 mm and a length of 7 mm. Water droplets were slides down in an orthogonal direction to the reverse-tapered uniaxial grooves. Sliding was defined to occur if the distilled water droplet moved more than 3 mm from its original position. Droplets were released onto samples from a height of 10 mm [26].

Statistical Analysis

All analyses were performed using the Statistical Package for Social Sciences (SPSS) version 25 (Advanced Analytics, Inc., Tokyo, Japan). Unless stated otherwise, all data were expressed as means \pm standard deviations (SDs).

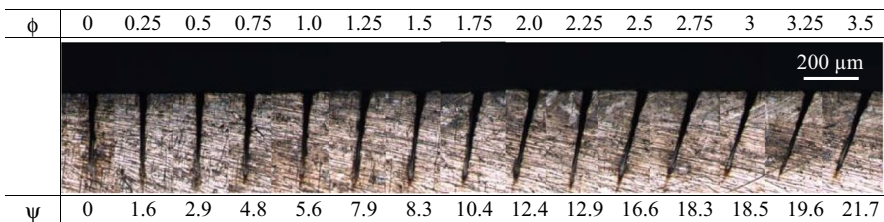
Results and Discussion

Characteristics of Optical Unit for Reverse-Taper Processing

Firstly, grooves with reverse-taper angles were fabricated by laser drilling using the optical unit for reverse-taper processing. The processing conditions were $11.6 \mu\text{m}$ of spot diameter, 250 mJ/mm^2 of fluence, 250 of shots, and 99.6% of the overlap ratio. Figure 3 shows the relationship between processed angle, ψ , and step mirror angle, ϕ , when reverse-tapered uniaxial grooves were processed using the femtosecond-pulsed laser with the fabricated optical unit by changing the step mirror angle in 0.25° increments over the range of $\pm 3.5^\circ$. It was revealed that the processed angle can be controlled linearly with the step mirror angles as follows:

$$\psi = 6.15 \phi \quad (^\circ) \quad (3)$$

A Side-views of processed reverse-tapered grooves



B Relationship between processed angle and step mirror angle

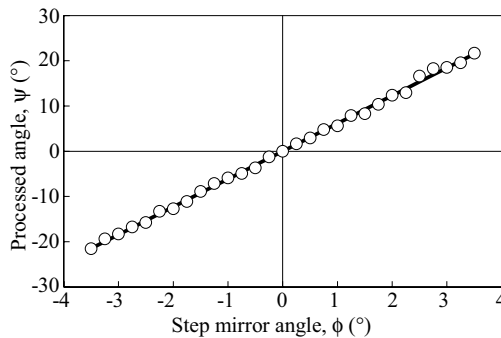


Fig. 3 Characteristics of reverse-tapered grooves processed using femtosecond-pulsed laser with fabricated optical unit

where, the coefficient of determination, R^2 , reached 0.998. The aspect ratio (ratio of depth-to-groove width, d/f_2) of the reverse-tapered uniaxial grooves was 6.35 ± 1.05 .

Optimization of Laser Processing

The depth was increased in proportion to the number of shots of perpendicularly uniaxial grooves when 250 mJ/mm^2 of fluence and 80% of overlap ratio were used (Fig. 4). It was revealed that the depth can be proportionally increased up to $25.4 \mu\text{m}$ by setting the number of shots to 15.

Measurement of Apparent Contact Angle and Sliding Characteristics

Four types of test-pieces with re-entrant textures were fabricated with the processed reverse-tapered angles of $5 - 20^\circ$. Here, the lateral surface geometries of the test-pieces were observed using a scanning electron microscope (SEM; JSM-6010LA, JEOL Ltd., Tokyo, Japan). The processed angle showed a reverse-taper ($\psi = 20^\circ$, Fig. 5A), and the pitch of the periodic structures was $\tau = 40.1 \pm 1.1 \mu\text{m}$ and the groove width was $f_2 = 29.4 \pm 2.3 \mu\text{m}$, respectively (Fig. 5B). Multiple linear grooves were observed to align independently without interfering. The groove width (f_2)/pitch (τ) ratio was obtained by dividing f_2 by τ . The f_2/τ ratio of 5, 10, 15, and 20° were 0.72, 0.71, 0.75, and 0.73, respectively. No significant difference was observed in the f_2/τ ratio.

Figure 6 shows the measured results of apparent contact angles, θ' , in two directions for each processed angle. The pitch and depth of each condition ranged between 40.1 and $40.4 \mu\text{m}$ and 27.8 and $33.1 \mu\text{m}$, respectively. No significant difference was observed in the pitch and depth for each condition. When the irradiation of femtosecond-pulsed laser, the ultra-short duration of the pulses leads the vaporization of the material under the effect of the huge instantaneous power received by the irradiated zone [27]. The iron-oxide layer will be disappeared when iron is processed with a femtosecond-pulsed laser [28]. However, when the sample is exposed

Fig. 4 Relationship between depth and number of shots (fluence: 250 mJ/mm^2 , OR: 80%)

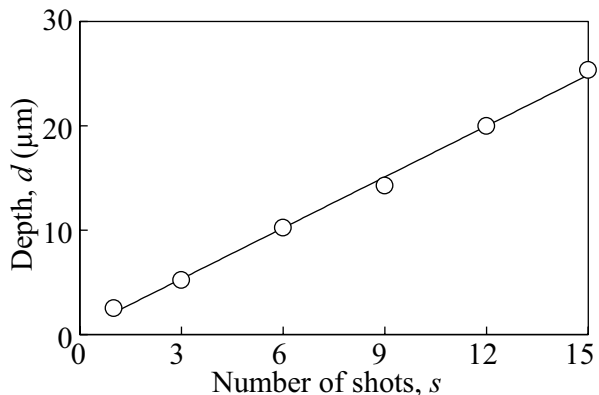
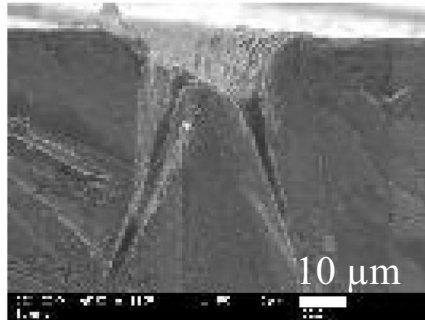
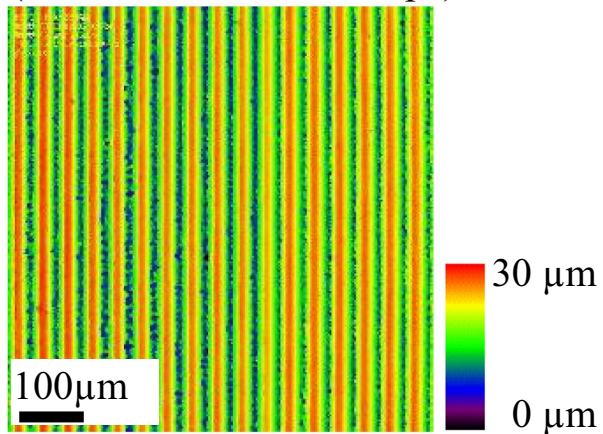


Fig. 5 Surface morphology of fabricated re-entrant textures on a stainless steel ($\psi=20^\circ$, test-piece with reverse-tapered grooves at 0° and $\pm 20^\circ$)

A Side view of reentrant structure (SEM)



B Top view of reentrant structure (laser confocal microscope)



to the atmosphere, oxidation starts again immediately after that, and an iron-oxide layer is formed quickly. The apparent contact angles were measured one week after laser processing because it has been reported that the laser processing of metal surfaces creates preferential sites for the adsorption of organic compounds from the air and that the wetting behavior changes with the amount of carbon on the structured surface [29, 30]. The apparent contact angle of the flat plate showed 103.7° and this water repellency was considered to be caused by surface oxidation. It was observed in the re-entrant texture that the apparent contact angle exhibited an increase with the processed angle. These results were entirely consistent with those of a previous report that the hydrophobicity of surface with re-entrant texture increases in proportion to the reverse-taper angle [31, 32]. In particular, the maximum apparent contact angle of the re-entrant texture reached 140.1° compared with 103.7° for the flat plate, regardless of observation direction. The re-entrant textures with reverse-tapered uniaxial grooves showed improvements the hydrophobicity 35% in maximum. As the

A Goniometer images

ψ	Flat plate	5	10	15	20
x	 $103.7 \pm 5.9^\circ$	 $116.4 \pm 1.8^\circ$	 $107.5 \pm 2.5^\circ$	 $116.4 \pm 2.9^\circ$	 $128.2 \pm 2.6^\circ$
y		 $133.4 \pm 3.5^\circ$	 $133.1 \pm 4.3^\circ$	 $134.5 \pm 3.7^\circ$	 $140.1 \pm 2.4^\circ$
Pitch τ (μm)		40.2 ± 2.1	40.1 ± 1.6	40.4 ± 1.6	40.1 ± 1.1
Depth d (μm)		33.1 ± 4.2	29.8 ± 4.2	27.8 ± 2.3	31.1 ± 4.4

B Measured results

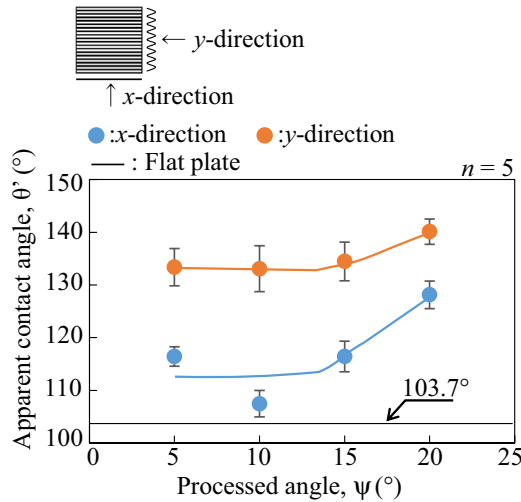


Fig. 6 Measured results of apparent contact angles of distilled water for re-entrant textures

theoretical development of the re-entrant texture, Tuteja et al. proposed an equation for shape and hydrophobicity [7], Chhatre et al. discussed the effect of the tooth width/groove width ratio [8], Wu and Suzuki presented the pinning and suspending condition for the theoretical development of the re-entrant texture [9], which led to suspending force by Liu et al. [33]. Thus, if the suspending force is sufficient, the droplet will not reach the bottom. These results showed that the water droplet did not reach the bottom of the re-entrant texture because it was sufficiently suspended to exceed the depth. It has also been reported that periodic structures applied in a uni-axial direction affect the apparent contact angles by less than 2% [34]. Our results were thus consistent with those of the previous report. Furthermore, the apparent contact angle in x- and y-directions presented different changing trend with the processed angle especially at 10°. The surface roughness, R_a , of the convex parts of

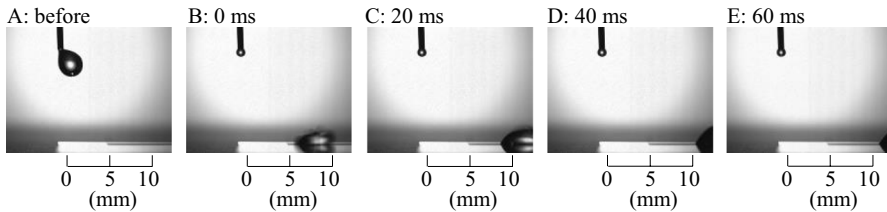


Fig. 7 Measured results of sliding characteristics for reentrant structures (test-piece with reverse-tapered grooves at 20°)

the grooves in y -direction with angles of 5° , 10° , 15° , and 20° were $0.51 \pm 0.03 \mu\text{m}$, $0.47 \pm 0.04 \mu\text{m}$, $0.52 \pm 0.02 \mu\text{m}$, and $0.54 \pm 0.03 \mu\text{m}$, respectively. The smoothness of the convex parts has a possibility to provide slight hydrophilicity.

On the flat sample of stainless steel, water droplets did not slide down even if the tilted angle exceeded 60° . In contrast, on test-pieces with re-entrant texture at the processed angle of 20° , water droplets slipped at $\alpha = 35^\circ$ (Fig. 7). The sliding velocity reached a maximum of 131 mm/s showing that the water droplets pass the processing length of 7 mm within 53 ms .

A limitation to our study was that stainless steel was used as the material for fabricating the re-entrant textures. The femtosecond-pulsed laser micropatterning has been applied to several metals such as titanium [35] and aluminum [36], and other materials as silicon [37] and polymer [38]. In future work, we intend to examine the application of re-entrant texture processing to various materials.

Conclusions

We have demonstrated a possibility of direct processing method of microscale re-entrant textures with arbitrary pitch and depth by using a femtosecond-pulsed laser. A direct fabrication method of re-entrant textures with reverse-tapered uniaxial grooves was proposed demonstrating improvements the hydrophobicity 35% in maximum. A maximum reverse-taper angle of 20° was achieved which can be controlled linearly via the step mirror angles of a fabricated optical unit. The re-entrant structures on stainless steel achieved the hydrophobicity over 140° of apparent contact angle with good stability allowing water droplets to slide off.

Since this method can be applied to additional processing to the products, the proposed methodology outlined herein may be adapted to applications in the medical field, semiconductor industry, automobile industry, or aviation industry. The apparent contact angle about 140° is not good enough expected for re-entrant structure. In future work, we would like to improve this method for applications involving biaxial grooves and laser drilling.

Supplementary Information The online version contains supplementary material available at <https://doi.org/10.1007/s40516-022-00198-y>.

Authors' Contribution **Masaki Yamaguchi:** Conceptualization, Investigation, Methodology, Supervision, Data curation, and Writing. **Shunichi Kato:** Laser processing and Measurement.

Funding This research was supported in part by grant no. 20H04514 from the Japan Society for the Promotion of Science, and was based on the ultra-sensitive and rapid cancer testing technique based on fiber-type amplification (Principal Investigator: M. Yamaguchi).

Declarations

Competing Interest The authors declare that they have no known competing financial interests or personal relationships that could have appeared to influence the work reported in this paper.

Open Access This article is licensed under a Creative Commons Attribution 4.0 International License, which permits use, sharing, adaptation, distribution and reproduction in any medium or format, as long as you give appropriate credit to the original author(s) and the source, provide a link to the Creative Commons licence, and indicate if changes were made. The images or other third party material in this article are included in the article's Creative Commons licence, unless indicated otherwise in a credit line to the material. If material is not included in the article's Creative Commons licence and your intended use is not permitted by statutory regulation or exceeds the permitted use, you will need to obtain permission directly from the copyright holder. To view a copy of this licence, visit <http://creativecommons.org/licenses/by/4.0/>.

References

1. Herminghaus, S.: Roughness-induced non-wetting. *Europhys Lett.* **52**, 165 (2000). <https://doi.org/10.1209/0295-5075/79/59901>
2. Cao, L., Hu, H.H., Gao, D.: Design and fabrication of micro-textures for inducing a superhydrophobic behavior on hydrophilic materials. *Langmuir* **23**(8), 4310–4314 (2007). <https://doi.org/10.1021/la063572r>
3. Tuteja, A., Choi, W., Ma, M., Mabry, J.M., Mazzella, S.A., Rutledge, G.C., McKinley, G.H., Cohen, R.E.: Designing superoleophobic surfaces. *Science* **318**, 1618–1622 (2007). <https://doi.org/10.1126/science.1148326>
4. Extrand, C.W.: Model for contact angles and hysteresis on rough and ultraphobic surfaces. *Langmuir* **18**(21), 7991–7999 (2002). <https://doi.org/10.1021/la025769z>
5. Nosonovsky, M.: Multiscale roughness and stability of superhydrophobic biomimetic interfaces. *Langmuir* **23**(6), 3157–3161 (2007). <https://doi.org/10.1021/la062301d>
6. Tuteja, A., Choi, W., Mabry, J.M., McKinley, G.H., Cohen, R.E.: Robust omniphobic surfaces. *Proc Natl Acad Sci USA.* **105**(47), 18200–18205 (2008). <https://doi.org/10.1073/pnas.0804872105>
7. Tuteja, A., Choi, W., McKinley, G.H., Cohen, R.E., Rubner, M.F.: Design parameters for superhydrophobicity and superoleophobicity. *MRS Bull.* **33**, 752–758 (2008). <https://doi.org/10.1557/mrs2008.161>
8. Chhatre, S.S., Choi, W., Tuteja, A., Park, K.C.K., Mabry, J.M., McKinley, G.H., Cohen, R.E.: Scale dependence of omniphobic mesh surfaces. *Langmuir* **26**(6), 4027–4035 (2010). <https://doi.org/10.1021/la903489r>
9. Wu, T., Suzuki, Y.: Design, microfabrication and evaluation of robust high-performance superlyophobic surfaces. *Sens Actuators B Chem.* **156**(1), 401–409 (2011). <https://doi.org/10.1016/j.snb.2011.04.065>
10. Kang, S.M., Choi, J.S.: Selective liquid sliding surfaces with springtail-inspired concave mushroom-like micropillar arrays. *Small* **16**, e1904612 (2020). <https://doi.org/10.1002/sml.201904612>
11. Wilke, K.L., Preston, D.J., Lu, Z., Wang, E.N.: Toward condensation-resistant omniphobic surfaces. *ACS Nano* **12**, 11013–11021 (2018). <https://doi.org/10.1021/acsnano.8b05099>
12. Yun, G.T., Jung, W.B., Oh, M.S., Jang, G.M., Baek, J., Kim, N.I., Im, S.G., Jung, H.T.: Springtail-inspired superomniphobic surface with extreme pressure resistance. *Sci Adv.* **4**, eaat4978 (2018). <https://doi.org/10.1126/sciadv.aat4978>

13. Dufour, R., Perry, G., Harnois, M., Coffinier, Y., Thomy, V., Senez, V., Boukherroub, R.: From micro to nano reentrant structures: hysteresis on superomniphobic surfaces. *Colloid Polym Sci.* **291**, 409–415 (2013). <https://doi.org/10.1007/s00396-012-2750-7>
14. Choi, H.J., Choo, S., Shin, J.H., Kim, K.I., Lee, H.: Fabrication of superhydrophobic and oleophobic surfaces with overhang structure by reverse nanoimprint lithography. *J Phys Chem C.* **117**, 24354–24359 (2013). <https://doi.org/10.1021/jp4070399>
15. Yamaguchi, M.: Microfabrication of re-entrant surface with hydrophobicity/oleophobicity for liquid foods. *Sci Rep.* **10**, 2250 (2020). <https://doi.org/10.1038/s41598-020-59149-2>
16. Wang, H., Zhang, Z., Wang, Z., Zhao, J., Liang, Y., Li, X., Ren, L.: Improved dynamic stability of superomniphobic surfaces and droplet transport on slippery surfaces by dual-scale re-entrant structures. *Chem Eng J.* **394**, 124871 (2020). <https://doi.org/10.1016/j.cej.2020.124871>
17. Kwon, M.H., Shin, H.S., Chu, C.N.: Fabrication of a super-hydrophobic surface on metal using laser ablation and electrodeposition. *Appl Surf Sci.* **288**, 222–228 (2014). <https://doi.org/10.1016/j.apsusc.2013.10.011>
18. Yang, Y., Zhang, Y., Hu, Y., Li, G., Zhang, C., Song, Y., Li, L., Ni, C., Dai, N., Cai, Y., Li, J., Wu, D., Chu, J.: Femtosecond laser regulated ultrafast growth of mushroom-like architecture for oil repellency and manipulation. *Nano Lett.* **21**, 9301–9309 (2021). <https://doi.org/10.1021/acs.nanolett.1c03506>
19. Torres-Peiró, S., González-Ausejo, J., Mendoza-Yero, O., Mínguez-Vega, G., Lancis, J.: Parallel laser micromachining based on diffractive optical elements with dispersion compensated femtosecond pulses. *Appl Surf Sci.* **21**(26), 31830–31836 (2013). <https://doi.org/10.1364/OE.21.031830>
20. Li, M.T., Liu, M., Sun, H.B.: Surface nanostructuring via femtosecond lasers. *Phys Chem Chem Phys.* **21**(44), 24262–24268 (2019). <https://doi.org/10.1039/c9cp05351d>
21. Nakata, Y.: Interference laser processing. *Adv Opt Techn.* **5**, 29–38 (2016). <https://doi.org/10.1515/aot-2015-0060>
22. Simon, P., Ihlemann, J.: Machining of submicron structures on metals and semiconductors by ultra-short UV-laser pulses. *Appl Phys A.* **63**, 505–508 (1996). <https://doi.org/10.1007/BF01571681>
23. Fan, Y., Wu, P., Baba, M.A., Luo, Q., Zhou, Q., Deng, G., Song, H., Wang, Y.: Improvement of the taper degree of laser-drilled holes via a double-pulse train. *Appl Opt.* **58**(26), 7028–7034 (2019). <https://doi.org/10.1364/AO.58.007028>
24. Cardoso, J.T., Aguilar-Morales, A.I., Alamri, S., Huerta-Murillo, D., Cordovilla, F., Lasagni, A.F., Ocaña, J.L.: Superhydrophobicity on hierarchical periodic surface structures fabricated via direct laser writing and direct laser interference patterning on an aluminium alloy. *Opt Lasers Eng.* **111**, 193–200 (2018). <https://doi.org/10.1016/j.optlaseng.2018.08.005>
25. Bradley, D., Sheppard, C.G.W., Suardjaja, I.M., Woolley, R.: Fundamentals of high-energy spark ignition with lasers. *Combust Flame.* **138**, 55–77 (2004). <https://doi.org/10.1016/j.combustflame.2004.04.002>
26. Zimmermann, J., Seeger, S., Reifler, F.A.: Water shedding angle: A new technique to evaluate the water-repellent properties of superhydrophobic surfaces. *Text Res J.* **79**, 1565–1570 (2009). <https://doi.org/10.1177/0040517509105074>
27. Mourier, L., Mazuyer, D., Lubrecht, A.A., Donnet, C., Audouard, E.: Action of a femtosecond laser generated micro-cavity passing through a circular EHL contact. *Wear.* **264**(5–6), 450–456 (2008). <https://doi.org/10.1016/j.wear.2006.08.037>
28. Raillard, B., Gouton, L., Ramos-Moore, E., Grandthyll, S., Müller, F., Mücklich, F.: Ablation effects of femtosecond laser functionalization on steel surfaces. *Surf Coat Technol.* **207**, 102–109 (2012). <https://doi.org/10.1016/j.surfcoat.2012.06.023>
29. Jagdheesh, R., García-Ballesteros, J.J., Ocaña, J.L.: One-step fabrication of near superhydrophobic aluminum surface by nanosecond laser ablation. *Appl Surf Sci.* **374**, 2–11 (2016). <https://doi.org/10.1016/j.apsusc.2015.06.104>
30. Kietzig, A.M., Mirvakili, M.N., Kamal, S., Englezos, P., Hatzikiriakos, S.G.: Laser-patterned superhydrophobic pure metallic substrates: cassie to wenzel wetting transitions. *J Adhes Sci Technol.* **25**, 2789–2809 (2011)
31. Brown, P.S., Bhushan, B.: Durable, superoleophobic polymer-nanoparticle composite surfaces with re-entrant geometry via solvent-induced phase transformation. *Sci Rep.* **6**, 21048 (2016). <https://doi.org/10.1038/srep21048>
32. Nosonovsky, M., Bhushan, B.: Why re-entrant surface topography is needed for robust oleophobicity. *Philos Trans A Math Phys Eng Sci.* **374**, 20160185 (2016). <https://doi.org/10.1098/rsta.2016.0185>

33. Liu, T., Kim, C.J.: Turning a surface superrepellent even to completely wetting liquids. *Science* **346**(6213), 1096–1100 (2014). <https://doi.org/10.1126/science.1254787>
34. Yamaguchi, M., Sasaki, S., Suzuki, S., Nakayama, Y.: Injection-molded plastic plate with hydrophobic surface by nanoperiodic structure applied in uniaxial direction. *J Adhes Sci Technol.* **29**, 24–35 (2014). <https://doi.org/10.1080/01694243.2014.973158>
35. Chen, F., Zhang, D., Yang, Q., Wang, X., Dai, B., Li, X., Hao, X., Ding, Y., Si, J., Hou, X.: Anisotropic wetting on microstrips surface fabricated by femtosecond laser. *Langmuir* **27**(1), 359–365 (2011). <https://doi.org/10.1021/la103293j>
36. Jang, M.Y., Kim, C.J., Park, J.W., Baek, S.Y., Kim, T.W.: Fabrication of Superhydrophobic Surface with Curved Grooves Using High Power Diode Laser. *J Nanosci Nanotechnol.* **21**(9), 4968–4973 (2021). <https://doi.org/10.1166/jnn.2021.19265>
37. Wang, M., Long, J., Liu, Y., Wang, N., Li, H., Yang, H., Ruan, S.: A Superhydrophilic Silicon Surface Enhanced by Multiscale Hierarchical Structures Fabricated by Laser Direct Writing. *Langmuir* **38**(36), 11015–11021 (2022). <https://doi.org/10.1021/acs.langmuir.2c01633>
38. Toosi, S.F., Moradi, S., Ebrahimi, M., Hatzikiriakos, S.G.: Microfabrication of polymeric surfaces with extreme wettability using hot embossing. *Appl Surf Sci.* **378**, 426–434 (2016). <https://doi.org/10.1016/j.apsusc.2016.03.116>

Publisher's Note Springer Nature remains neutral with regard to jurisdictional claims in published maps and institutional affiliations.